Available online at www.sciencedirect.com
ScienceDirect
Planetary and Space Science 55 (2007) 89–99
Planetary and Space Science
www.elsevier.com/locate/pss

Io–Jupiter interaction, millisecond bursts and field-aligned potentials

S. Hess[a,b,*], P. Zarka[a], F. Mottez[c]

[a]Observatoire de Paris—LESIA/CNRS, 5 Place J. Janssen, 92195 Meudon Cedex, France
[b]CETP/CNRS, 78140 Vélizy, France
[c]Observatoire de Paris—LUTH/CNRS, 5 Place J. Janssen, 92195 Meudon Cedex, France

Received 1 December 2005; received in revised form 12 May 2006; accepted 12 May 2006
Available online 13 July 2006

Abstract

Jovian millisecond (or S-) bursts are intense impulsive decametric radio bursts drifting in frequency in tens of milliseconds. Most of the theories about their origin comprise an interpretation of their frequency drift. Previous analyses suggest that S-bursts are cyclotron-maser emission in the flux tubes connecting Io or Io's wake to Jupiter. Electrons are thought to be accelerated from Io to Jupiter. Near Jupiter, a loss cone appears in the magnetically mirrored electron population, which is able to amplify extraordinary (X) mode radio waves. Here, we perform an automated analysis of 230 high-resolution dynamic spectra of S-bursts, providing 5×10^6 frequency drift measurements. Our data are consistent with the above scenario. In addition, we confirm over a large number of measurements that the frequency drift $\mathrm{d}f/\mathrm{d}t(f)$ is in average negative and decreases (in absolute value) at high frequencies, as predicted by the adiabatic theory. We find a typical energy of 4 keV for the emitting electrons. In 15% of the cases (out of 230), we find for the first time evidence of localized ~1 keV electric potential jumps at high latitudes along the field lines connecting Io or Io's wake to Jupiter. These potential jumps appear stable over tens of minutes. Finally, a statistical analysis suggests the existence of a distributed parallel acceleration of the emitting electrons along the same field lines.

Keywords: Jupiter–Io interaction; S-bursts; Radio emissions; Electrons acceleration; Potential drops

1. Introduction

Jupiter is an intense decametric radiation source. Some of these emissions are recorded on Earth for particular Io-phases (i.e. Observer–planet–satellite angle) (Carr et al., 1983) and are due to the Io–Jupiter interaction (Queinnec and Zarka, 1998; Saur et al., 2004). While Io follows a keplerian orbit around the planet with a period of 42 h 27.5 min, the Io torus is dragged by the Jupiter magnetic field with a period nearly equal to the planetary rotation period (9 h 55.5 min). An electric field results from the velocity of the torus magnetized plasma in the Io frame ($E=-v\times B$). This electric field induces currents and/or Alfvén waves (Goldreich and Lynden-Bell, 1969; Neubauer, 1980; Saur, 2004) which accelerate electrons from the Io torus toward Jupiter along the magnetic field lines. The magnetic mirror at the foot of the Io flux tube (IFT) reflects a part of the electrons, whose distribution is then unstable relative to the cyclotron-maser instability and produces emission at the local cyclotron frequency (Wu and Lee, 1979; Louarn, 1992).

Some of these radio emissions are called millisecond or short (S-) bursts, due to their time scale and their discrete impulsive nature. Fig. 1a shows an example of S-burst dynamic spectrum. The S-bursts present most of time a negative drift in the time–frequency plane. This drift was interpreted by Ellis (1965, 1974) as a radio source motion consistent with the electron adiabatic motion. Since the electrons emit at the local cyclotron frequency and because of the negative drift, the emitting electrons must be reflected electrons, going from Jupiter to Io. This model still requires a definitive validation. This is the first objective of the present study.

Moreover, S-bursts shape studies have shown the presence of breaks of the bursts drift in the time–frequency plane (Riihimaa, 1991). We consider that such structures

*Corresponding author. Observatoire de Paris—LESIA/CNRS, 5 Place J. Janssen, 92195 Meudon Cedex, France. Tel.: +33 1 45 07 76 98.
E-mail address: sebastien.hess@obspm.fr (S. Hess).

0032-0633/$ - see front matter © 2006 Elsevier Ltd. All rights reserved.
doi:10.1016/j.pss.2006.05.016

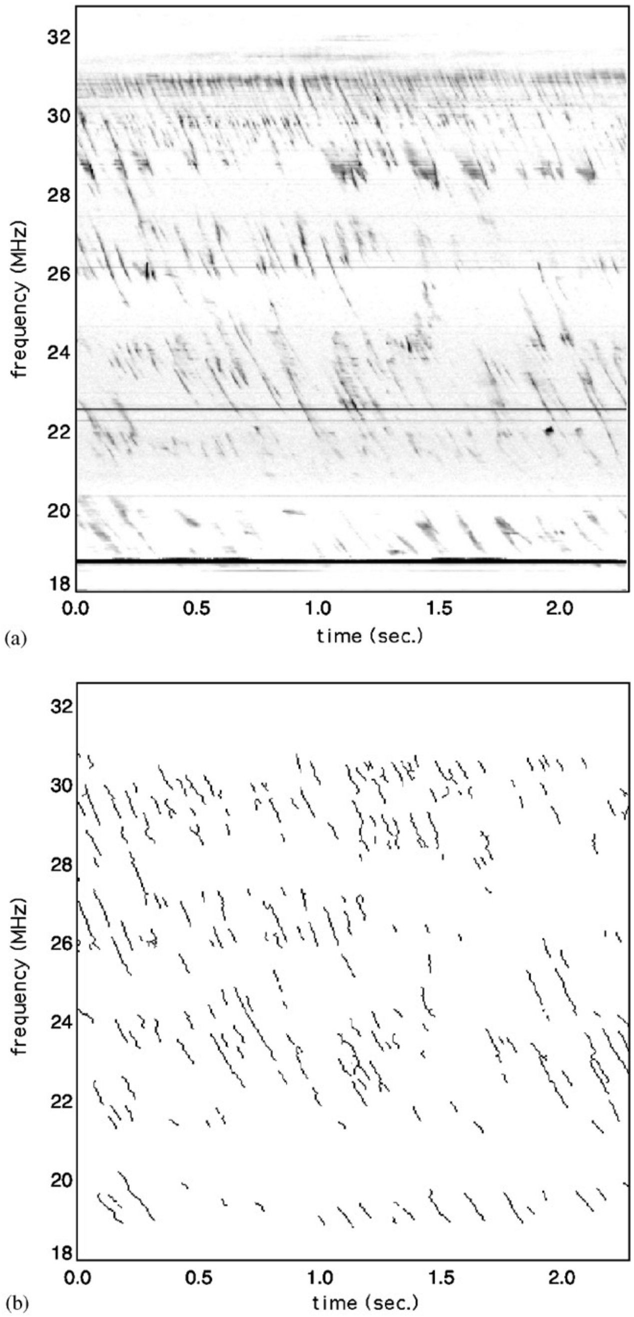

Fig. 1. (a) Example of dynamic spectrum showing Jovian S-bursts during 2.2 s in the range 18–32 MHz. It was recorded at the Nançay decameter array with a resolution of 3 ms × 50 kHz on 95/04/07. Tilted structures are S-bursts, whereas horizontal lines are interference. (b) The same dynamic spectrum, after analysis by the recognition software. Each burst is identified as a separate entity and its skeleton is computed.

could be due to the presence of accelerating or decelerating structures along the IFT. Our second objective is to identify and study these structures.

The emission processes are not discussed in this paper. We study the electron motion and the presence of acceleration structure along the IFT. We present the adiabatic model in Section 2, and the observations in Section 3. In Section 4 we discuss the validity of the adiabatic model. Section 5 presents the observation of accelerating structures in the observed frequency range. Section 6 is a statistical study of the emitting electrons characteristics suggesting acceleration outside the observed frequency range.

2. Adiabatic model

2.1. Definitions

The adiabatic model was proposed as an explanation of the generally negative drift rates of the S-bursts in the time–frequency plane. In this model the emission is due to electrons reflected by magnetic mirror effect (at a local cyclotron frequency called the mirror frequency f_{mirror}) and emitting along the field line at the local cyclotron frequency f_{ce}. The drift rate $\mathrm{d}f/\mathrm{d}t$ of the S-bursts in the time–frequency frame is connected to the motion of the emitting electrons by

$$\frac{\mathrm{d}f}{\mathrm{d}t} = \frac{\mathrm{d}f_{\mathrm{ce}}}{\mathrm{d}s}\frac{\mathrm{d}s}{\mathrm{d}t} = \frac{\mathrm{d}f_{\mathrm{ce}}}{\mathrm{d}s}\, v_{\parallel}(f_{\mathrm{ce}}), \tag{1}$$

where $v_{\parallel}$ is the radio source (i.e. the emitting electrons) parallel velocity, chosen to be positive for up-going electrons. $\mathrm{d}f_{\mathrm{ce}}/\mathrm{d}s$ is directly deduced from the Jovian magnetic field model and $v_{\parallel}(f_{\mathrm{ce}})$ is deduced from the first adiabatic invariant conservation. We consider here that the motion is adiabatic as long as the first adiabatic invariant μ is conserved

$$\mu = v_{\perp}^2(f_{\mathrm{ce}})/f_{\mathrm{ce}} = v^2(f_{\mathrm{mirror}})/f_{\mathrm{mirror}}, \tag{2}$$

where v is the electrons velocity, f_{ce} the local cyclotron frequency and f_{mirror} the cyclotron frequency at which electrons are reflected. In the case of an adiabatic motion without acceleration, v^2 is constant along the trajectory. But this definition of adiabaticity permits the presence of parallel accelerations by electric fields.

2.2. Magnetic field models

The magnetic field model is used to compute the parallel velocity of the radio source from the drift rate measurements (Eq. (1)). Moreover, it gives the relation between the Jovicentric coordinates of the source and the local cyclotron frequency.

The magnetic model used in previous papers was a dipolar magnetic field model, since it permits analytical computation of the drift rate. Nevertheless, the Jupiter magnetic field has strong multipolar components and thus, the maximum field strength at the surface of Jupiter is larger than the one given by the Jovian dipolar moment ($4.2G.R_{\mathrm{J}}^3$). Zarka et al. (1996) introduced a dipolar magnetic field model with a moment equal to $7G.R_{\mathrm{J}}^3$. Since the magnetic field is independent of longitude in this model, we use it for studies of the drift rate averaged on all measurements.

A more accurate magnetic field model is VIP4 (Connerney et al., 1998) based on Voyager and Pioneer magnetometer measurements together with IR observation of the IFT footprint at the surface of Jupiter. It is expected to be the most accurate available model of the magnetic field along the IFT and its vicinity. We use it for studies of individual observations, for which we get the IFT longitude at the observation time.

2.3. Adiabatic motion without electric field

The adiabatic motion of the emitting electrons without acceleration by parallel electric fields is the baseline model proposed by Ellis (1965). Its main characteristic is the kinetic energy conservation along the electrons trajectory. It permits to write the electrons velocity as

$$v_\perp^2 = \mu f_{\rm ce} = v^2 \sin^2\alpha, \tag{3}$$

$$v_\parallel^2 = v^2 - \mu f_{\rm ce} = v^2 \cos^2\alpha, \tag{4}$$

where α is the pitch angle (i.e. the $\mathbf{v},\mathbf{B}$ angle). The equatorial pitch angle and the mirror frequency $f_{\rm mirror}$ are related by

$$\sin^2\alpha_{\rm eq} = f_{\rm eq}\mu/v^2 = f_{\rm eq}/f_{\rm mirror}, \tag{5}$$

where $f_{\rm eq}$ is the equatorial cyclotron frequency. Eqs. (3) and (4) show that the electrons motion is characterized by two parameters only, for example, their equatorial pitch angle $\alpha_{\rm eq}$ and their kinetic energy $W = (m/2)(v_\perp^2 + v_\parallel^2)$.

2.4. Representations

In previous papers (Zarka et al., 1996; Galopeau et al., 1999), drifts were studied and represented by the drift rate as a function of the frequency $({\rm d}f/{\rm d}t)(f)$, and then compared to the drift rate $({\rm d}f/{\rm d}t)(f_{\rm ce})$ predicted by the adiabatic model. The latter is a curve possessing a local maximum and a null value at the mirror frequency $f_{\rm mirror}$. Varying the equatorial pitch angle $\alpha_{\rm eq}$ shifts the mirror frequency, while varying the total kinetic energy W changes the amplitude of the drift rate. Fig. 2a shows the drift rate as a function of cyclotron frequency for adiabatic motion of the emitting electrons with different energies and equatorial pitch angles.

However, the adiabatic model is connected to the drift rate $({\rm d}f/{\rm d}t)(f)$ through the emitting electrons parallel velocity (Eq. (1)). Since the parallel kinetic energy is a linear function of the frequency (Eq. (4)), it is more interesting for an easier fitting of the data to deduce $v_\parallel$ from the measured drift rate and magnetic field and to represent the parallel kinetic energy $W_\parallel(f)$ instead of the drift rate $({\rm d}f/{\rm d}t)(f)$. Then an adiabatic motion is represented by a straight line, and the electrons characteristics appear more explicitly in this representation. The total kinetic energy is equal to the parallel kinetic energy at null frequency $W = W_\parallel(f=0)$. The slope of the line representing the parallel kinetic energy $W_\parallel(f)$ is equal to $-\mu$.

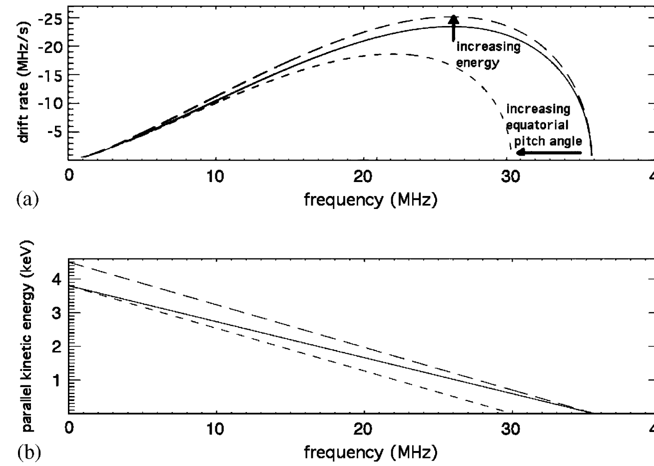

Fig. 2. (a) Drift rate as a function of frequency in the adiabatic model. Continuous line stand for $W = 3.8$ keV and $\alpha_{\rm eq} = 2.3°$, short discontinuous line for $W = 3.8$ keV and $\alpha_{\rm eq} = 2.5°$, long dashed line for $W = 4.5$ keV and $\alpha_{\rm eq} = 2.3°$. (b) Parallel kinetic energy $W_\parallel(f)$ for the adiabatic model. The parameters are the same as above.

Fig. 2b shows the parallel kinetic energy as a function of frequency for adiabatic motion of the emitting electrons for several energies and equatorial pitch angles. The decrease of the parallel kinetic energy is linear with frequency. Electrons with the same μ but with different energies and equatorial pitch angles follow parallel lines. As the graph depends on the cyclotron frequency $f_{\rm ce}$ and not on altitude, it is independent of the Jovian magnetic field model.

2.5. Adiabatic motion with a spatially distributed parallel electric field

The acceleration of the emitting electrons in adiabatic motion by a parallel electric field has been studied by Galopeau et al. (1999), under the assumption of a constant electric field along the magnetic field line, and using a dipolar magnetic field model. This case has no analytical solution in a realistic magnetic multipolar Jovian field model. However, the cyclotron frequency gradient ${\rm d}f_{\rm ce}/{\rm d}s$ varies slowly on the observed altitude range, so that a linear variation of the electric potential can be approximated by a potential proportional to the local electron cyclotron frequency. This assumption permits the analytical treatment below. The velocity of the emitting electrons is given by

$$v_\perp^2 = \mu f_{\rm ce}, \tag{6}$$

$$v_\parallel^2 = v_{f=0}^2 - \mu f_{\rm ce} + \frac{2e}{m_{\rm e}}\frac{{\rm d}\phi}{{\rm d}f_{\rm ce}} f_{\rm ce} = v_{f=0}^2 - (\mu - \varepsilon) f_{\rm ce}. \tag{7}$$

The parameter ε can be considered as the part of the rate of acceleration ${\rm d}v_\parallel^2/{\rm d}f_{\rm ce}$ due to a parallel electric field, and supposed here to be uniform. The drift $({\rm d}f/{\rm d}t)(f)$ has in this case the same shape as in the case without electric field, i.e. the parallel kinetic energy again depends linearly on the cyclotron frequency. But the electron velocities can no more be expressed as a function of their former total energy $W_{f=0}$ and equatorial pitch angle α_{eq} only. The mirror frequency is no more related to the equatorial pitch angle by Eq. (5), but

$$\alpha^2 \sim \tan^2(\alpha) = \frac{v_\perp^2}{v_\parallel^2} = \frac{\mu f_{ce}}{(\mu - \varepsilon)(f_{mirror} - f_{ce})}. \quad (8)$$

When we include a parallel electric field in the adiabatic model the pitch angle α depends on the first adiabatic invariant μ and then particles with the same equatorial pitch angles but different energies will have different mirror frequencies.

3. Observations

Analysis of S-Bursts drift rate was performed on 230 high-resolution dynamic spectra. They were recorded with an acousto-optical spectrograph at the Nancay decameter array (Boischot et al., 1980) in 1995 and 1996. This multichannel receiver records digital dynamic spectra with a time resolution of 3 ms and a frequency resolution of 50 kHz over 512 channel simultaneously (the total frequency range observed is 25 MHz). All the dynamic spectra have been recorded with right-handed polarization, which corresponds to emissions from the northern Jovian hemisphere. The Io phase and the central meridian longitude (CML) during the records correspond to the so-called "Io-B" source (Carr et al., 1983; Queinnec and Zarka, 1998).

Table 1 lists the number of dynamic spectra recorded for each day of observation. Each dynamic spectrum has a total duration of 20 s (6000 consecutive spectra).

The bursts were detected between ~12 MHz (the Earth's ionospheric cutoff) and ~37 MHz (maximum electron cyclotron frequency at the surface of Jupiter). This spectral range corresponds to an altitude range from the Jovian surface to $0.4R_J$ ($1R_J = 71,398$ km) above it.

We use a recognition software for the S-Bursts, which identifies each burst and computes its skeleton (LeGoff, 1999). Fig. 1 shows an example of dynamic spectrum analysis by this software. The S-bursts skeletons corresponding to the dynamic spectrum of Fig. 1a is shown in Fig. 1b. Then a linear regression is performed on each burst every 50 kHz over a frequency range of ±0.25 MHz to measure its drift rate as a function of frequency. Drift rate computation is validated with a burst "toy-model". The error on drift rate measurements was estimated to be ~1% RMS. It is much less than the intrinsic dispersion of drift rates at each frequency in a 20 s dynamic spectrum.

A detailed description of burst recognition and drift rate computation is presented in Appendix A.

Table 1
Number of dynamic spectra, adiabatic segments and potential drops for each day of observation

Day	Number of dynamic spectra	Number of adiabatic segments	Number of potential drops
06 April 95	6	9	2(*)
07 April 95	30	45	8
13 April 95	17	21	2
14 April 95	35	45	6
21 April 95	6	6	0
09 May 95	18	25	2
16 May 95	21	30	5
23 May 95	27	35	4
11 June 96	48	71	10(*)
19 June 96	7	7	0
26 June 96	15	15	0
Total	230	309	39

The (*) symbol indicates that a dynamic spectrum with two potential drops was recorded this day. There are often more adiabatic segments than their total (dynamic spectra + potential drops). The difference is due to the fact that some accelerations do not correspond to the criteria of potential drops.

4. Confirmation of the electron's adiabatic motion

4.1. Global analysis of all measurements

Fig. 3a shows the drift rates measurements made by Zarka et al. (1996) and before (see references therein). Drift rate measurements prior to 1996 have shown a drift rate $|(df/dt)(f)|$ increasing with the frequency. But observations beyond 34 MHz did not exist, and were very rare beyond 32 MHz, so that it was not possible to observe the decrease of $|(df/dt)(f)|$. Using for the first time an automated S-burst recognition software applied to a high-resolution (10 ms × 50 kHz) dynamic spectra, Zarka et al. (1996) performed 45 000 drift rate measurements including a few tens above 32 MHz. They could then observe for the first time the decrease of the drift rate $|(df/dt)(f)|$ at high frequencies, as predicted by the adiabatic model. Using a dipolar Jovian magnetic field model with a moment of $7G.R_J^3$, they found a mean total energy $W = 5.3 \pm 2.2$ keV and an equatorial pitch angle $\alpha_{eq} = 2.8°$ for the emitting electrons. They also observed an abrupt variation (increase) of the drift rate at about 22 MHz.

But the amount of data, especially beyond 32 MHz was limited, and these new results needed to be confirmed. Using a more accurate recognition software based on a different algorithm (see Appendix A), higher time resolution data (3 ms), and analyzing more observations, we have obtained about 5×10^6 drift rate measurements, including more than 2×10^5 above 32 MHz. Fig. 3b shows our drift rate measurements as a function of frequency. The continuous line is the average drift rate and the dashed ones the standard deviation. These drift rate measurements confirm

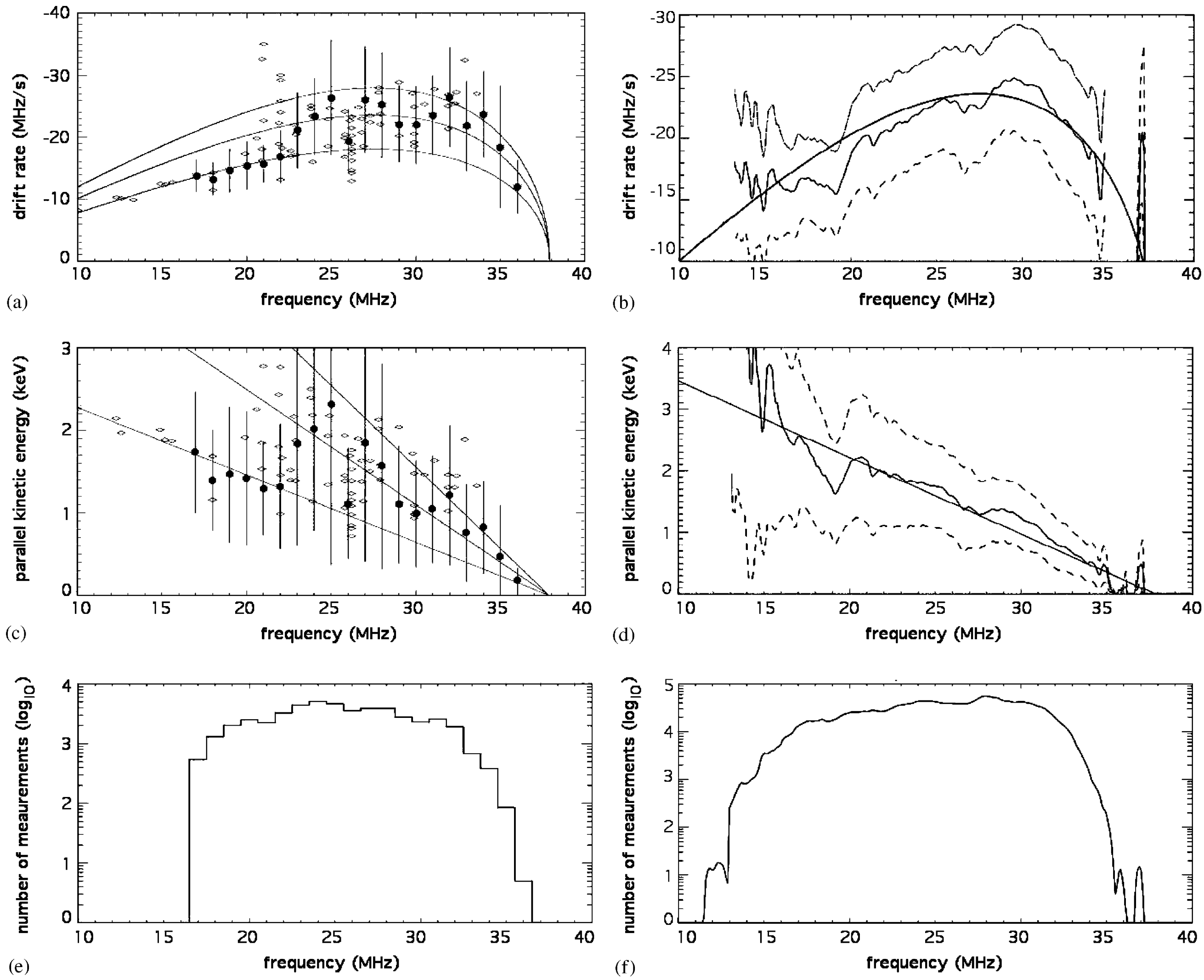

Fig. 3. (a) Previous drift rate measurements. Solid dots present the measurements made by Zarka et al. (1996) and open ones measurement made in previous papers. The three continuous lines show the adiabatic curve with $W = 5.3 \pm 2.2\,\mathrm{keV}$ and $\alpha_{eq} = 2.8°$. The same data are presented in the $W_\parallel(f)$ frame in (c). (b) Drift averaged on all our measurements. The dashed lines show the standard deviation. The drift decreases above 30 MHz. The continuous line shows the measured drift which is compatible with a drift computed for an adiabatic motion of the emitting electrons (bold line) with $\alpha_{eq} = 2.7°$ and $v = 0.13c$ in a dipolar magnetic field, as shown by (d) which presents the measurements in the $W_\parallel(f)$ frame. (e) Distribution of the number of measurements per 1 MHz frequency bin in Zarka et al. (1996). (f) Distribution of the number of measurements per 100 kHz frequency bin in our study. We get about 5×10^6 measurements between 12 and 37 MHz.

the decrease of the drift rate $|(\mathrm{d}f/\mathrm{d}t)(f)|$ above 30 MHz. The linear decrease of the parallel kinetic energy $W_\parallel$ with frequency shown by Fig. 3d is compatible with an adiabatic model, using the same dipolar model as above, with an electrons kinetic energy of $W = 4.5 \pm 1.1\,\mathrm{keV}$ and an equatorial pitch angle of $\alpha_{eq} = 2.7°$. This computed adiabatic drift rate is represented by the bold line in Figs. 3b–d. These values are consistent with those of Zarka et al. (1996). They strongly reinforce the conclusion that electrons have on the average an adiabatic motion along the IFT.

4.2. Analysis of individual dynamic spectra

The above global study on all the measurements gives results compatible with the adiabatic model, but the dispersion of drift rate measurements at each frequency is large (4 MHz/s at 1σ, shown in Fig. 3). This may be due to the spreading in time of the observations, mixing measurements of S-bursts with different characteristics. Thus, we analyze each individual dynamic spectrum, using the more accurate VIP4 magnetic field model (Connerney et al., 1998). An average drift rate is computed for each dynamic spectrum (of duration of 20 s) at each frequency. In the $W_\parallel(f)$ representation the adiabatic model predicts a linear decrease of $W_\parallel$ with the frequency. Fig. 4 shows two examples of the measured parallel kinetic energy as a function of the frequency. In Fig. 4a as in ~70% of the cases, the decrease in parallel kinetic energy versus frequency is approximately linear (i.e. compatible with the adiabatic model) over most of the frequency range.

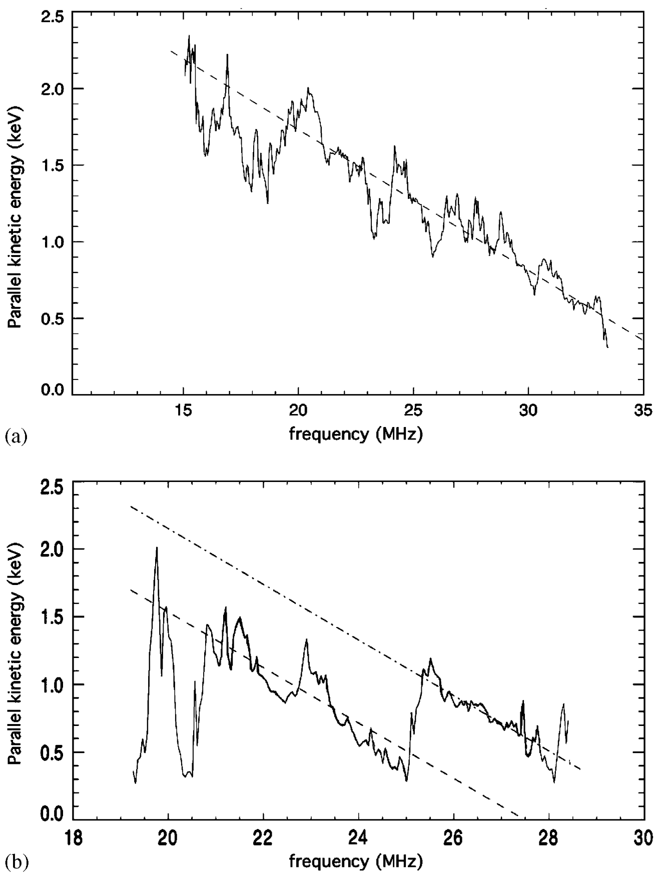

Fig. 4. Parallel kinetic energy function of frequency computed for an individual dynamic spectrum. The dashed lines show the slopes of the automatically recognized "adiabatic segments". (a) (observed on 07 April 95) The decrease is linear (compatible with the adiabatic model) on the whole frequency range. (b) (observed on 23 May 95) The decrease is linear on two frequency ranges (compatible with the adiabatic model with localized acceleration).

In addition, for 64 dynamic spectra the parallel kinetic energy decrease with frequency is linear in two frequency ranges (we call them "adiabatic segments") or more (nine dynamic spectra with three segments and three with four segments), suggesting the effect of localized potential drops superimposed on the adiabatic motion (see below). Fig. 4b shows an example of dynamic spectrum for which the parallel kinetic energy decreases linearly in two frequency ranges.

For each adiabatic segment, where the decrease of $W_{\parallel}$ is linear, we can derive the total energy and equatorial pitch angle of the electrons. Thus, we perform an automated recognition of the adiabatic segments. Each linear decrease of the parallel kinetic energy ($W_{\parallel}$) over more than 2 MHz is represented by a straight line segment. Those for which cross-correlation with the observations is more than 0.9 are recognized as adiabatic segments. Since there can be several segments per dynamic spectrum, the number of "adiabatic segments" is larger than the number of dynamic spectra (Table 1). Adiabatic segments represent ~80% of our 5×10^6 measurements. The 20% left correspond to noisy drift rates or acceleration ranges.

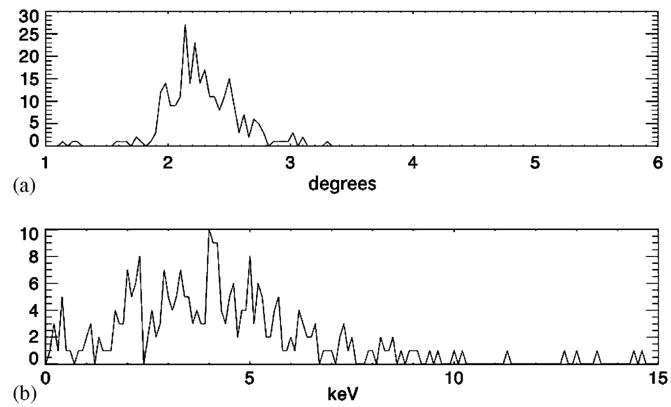

Fig. 5. (a) Histogram of the equatorial pitch angle of the electrons, computed for each "adiabatic segment" recognized. The mean equatorial pitch angle is 2.3°. (b) Histogram of the total energy of the emitting electrons, computed for each "adiabatic segment" recognized. The mean energy is 3.9 keV.

The total kinetic energy W and the equatorial pitch angle α_{eq} of the emitting electrons are computed for each adiabatic segment. The former are displayed in Fig. 5. The mean energy is found to be $W = 3.9 \pm 0.9$ keV, consistent with the previous studies and with the global analysis presented in Section 4.1.

Fig. 5a shows the equatorial pitch angle measurements whose mean value is found to be $2.3^\circ \pm 0.2^\circ$. It corresponds to a mirror frequency about 35 MHz, compatible with the maximum electron cyclotron frequency at the surface of Jupiter.

Moreover, Fig. 5a shows a cut-off equatorial pitch angle near 1.9°. This angle corresponds to a mirror frequency equal to 40 MHz (i.e. ~ the maximum cyclotron frequency at the surface of Jupiter). The absence of electrons with equatorial pitch angle lower than 1.9° corresponds to the presence of a "loss cone" due to the collisional loss in Jovian ionosphere of the electrons with mirror frequency larger than 40 MHz. Moreover, the electrons with equatorial pitch angle larger than about 3° are not observed, because their mirror frequency is below 12 MHz (atmospheric cut-off) and thus are not observable from the ground.

5. Potential drops

A potential drop implies a localized parallel acceleration. Since a parallel acceleration does not change the first adiabatic invariant, a potential drop corresponds to a localized transition between two parallel lines in the $W_{\parallel}(f)$ representation (Fig. 4b), i.e. a jump between two adiabatic segments . We found 64 dynamic spectra out of 230 presenting two or more "adiabatic segments". We define as a "localized potential drop" a transition whose length is less than 2 MHz between two "adiabatic segments" whose slopes differ by less than 40%. We detect 39 drops of parallel kinetic energy compatible with our definition of potential drops. They all correspond to downward acceleration. Table 1 presents the number of potential drops detected for each day of observation. Two dynamic spectra show two successive potential drops. The number of adiabatic segments in Table 1 is larger than the number of dynamic spectra plus the number of potential drops, because all accelerations are not potential drops. The excess of adiabatic segments corresponds to changes of adiabatic invariant μ (nonadiabatic acceleration) and/or smooth accelerations (whose "lengths" are >2 MHz).

Fig. 6a shows the distribution of the amplitudes of the drops. The mean amplitude is found to be 0.9 keV. As the noise inherent to the observations limits the detection of the weak amplitude drops, our statistics are probably biased for low values. The dispersion due to the finite resolution of dynamic spectra and to the measurement method is $\sim$0.1 keV on electrons energy measurements. It means that the decrease of the number of potential drops below 0.6 keV may be due to this detection limit.

The potential drops altitudes can be deduced from the radio frequency at which they occur because the emission is near the local electron cyclotron frequency, which depends on the distance from the planet. Fig. 6b shows the distribution in frequency of the potential drops. The detection range is limited from 14 to 33 MHz, due to the fact that we get drift rates measurements between 12 and 36 MHZ, and that we require a minimal length for adiabatic segments (2 MHz). However, 75% of the potential drops are localized between 22 and 28 MHz, i.e. at an altitude of about $0.1R_J$ above the planetary surface. It corresponds to the frequency range in which Zarka et al. (1996) observed abrupt variations of the drift rate which correspond to increases of the kinetic energy. Then these variations could be due to the presence of potential drops in their data, with characteristics similar to those we observe. Such variations do not appear in our global drift rate measurements (Fig. 3) because the drift rates are averaged over many more observations (230 dynamic spectra in our study, only 17 for Zarka et al., 1996).

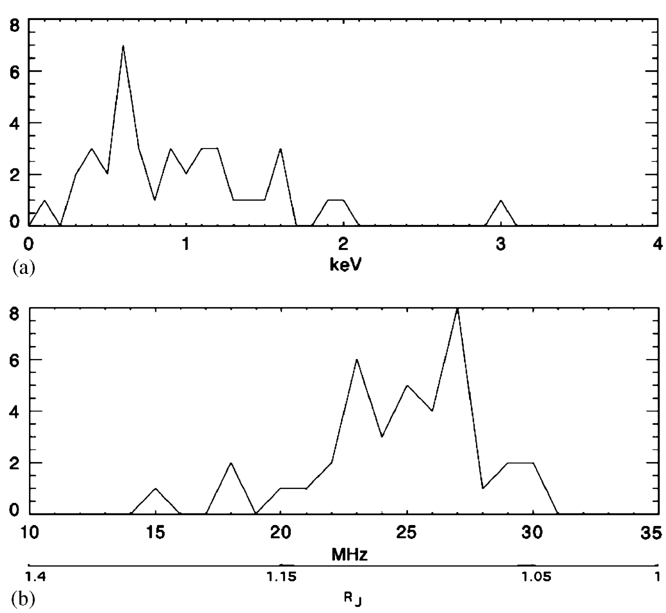

Fig. 6. (a) Histogram of the potential drops amplitudes. The mean amplitude is 0.9 keV. (b) Histogram of the potential drops localization. Seventy-five percents of the drops are localized between 22 and 28 MHz. Jovicentric distance is computed with the VIP4 model for a longitude of Io equal to 180°, which correspond to a Io-B source (Queinnec and Zarka, 1998).

Fig. 7 shows the localization of the potential drops in the time–frequency (or time-altitude) frame for the 3 days which present the most numerous potential drops observations. We study the evolution of the accelerating structures in time. We note that consecutive drops often have near by frequencies, suggesting that potential drops may be stable over timescales of minutes (for example, the two drops near 22 MHz on 96/06/11) to tens of minutes (for example, the three potential drops near 24 MHz on 95/04/14). The potential drops altitude can vary abruptly between two long-lived structures (e.g. on 96/06/11 $t \simeq 75$ min.).

6. Parallel acceleration

6.1. Energy decrease with frequency

As we compute the total energy W and the equatorial pitch angle α_{eq} on every frequency range corresponding to the adiabatic segments, it is possible to compute the average energy and equatorial pitch angle at each frequency. Fig. 8a shows the averaged equatorial pitch angle at each frequency $\langle\alpha_{eq}\rangle(f)$. It decreases with the frequency. The connection between the equatorial pitch angle and the mirror frequency (Eq. (5)) explains this decrease, since electrons with larger equatorial pitch angle are reflected at lower frequencies.

Fig. 8b shows that the averaged total kinetic energy $\langle W\rangle(f)$ decreases with frequency too. Without acceleration, there would not be any connection between energy and mirror frequency, and the energy would not follow the same tendency as the equatorial pitch angle.

With Fig. 9, we illustrate an interpretation in terms of downward parallel acceleration process introducing a relation between the total kinetic energy W (or μ as we will see) and the mirror frequency f_{mirror}. Electrons initially with the same pitch angle α_0 (i.e. the same mirror frequency $f_{m,0}$) but different kinetic energy (velocities $v_1 < v_2$) are subject to a parallel acceleration which adds the same parallel velocity $\delta v_{\parallel}$. The final pitch angles α_1 and α_2 of particles 1 (low energy) and 2 (high energy) follow the relation $\alpha_1 < \alpha_2$ (i.e. mirror frequencies $f_{m_1} > f_{m,2}$). A more careful examination of Fig. 9 shows that the dependence of the pitch angle is mainly due to the perpendicular part of the energy, that is proportional to the magnetic moment. This can be found analytically, by derivation of the relation

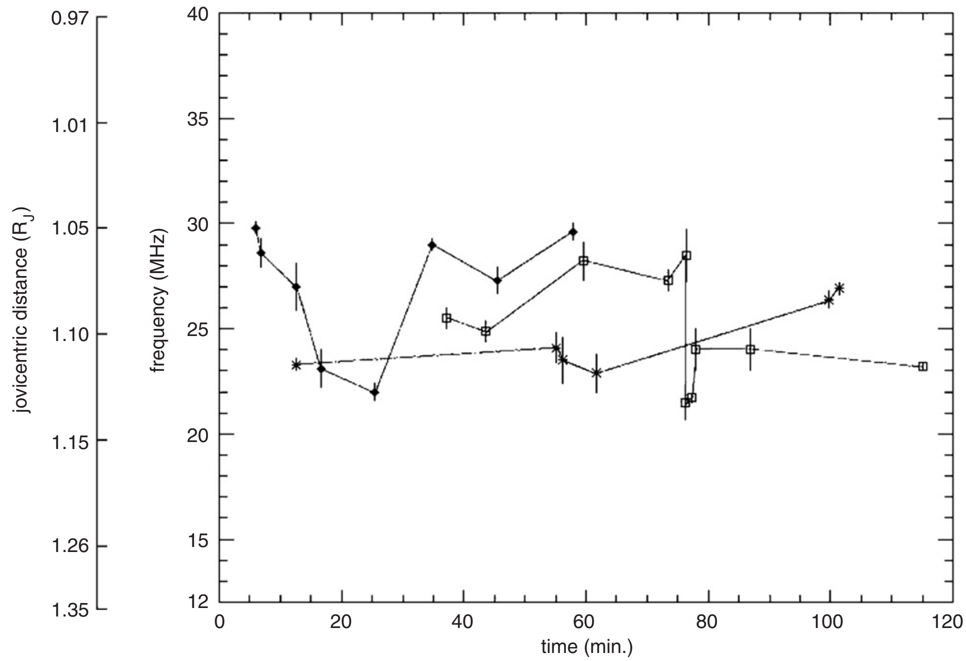

Fig. 7. Localization of the potential drops in the time–frequency frame for the 3 days which present the most observations. Dots stand for the observations of April 7th, 1995 from 4 h 20 min. Stars for observations of April 14th, 1995 from 4 h 25 min. Squares for observations of June 11th, 1996 from 22 h 40 min. Jovicentric distance is computed with the VIP4 model for a Io longitude equal to 180°.

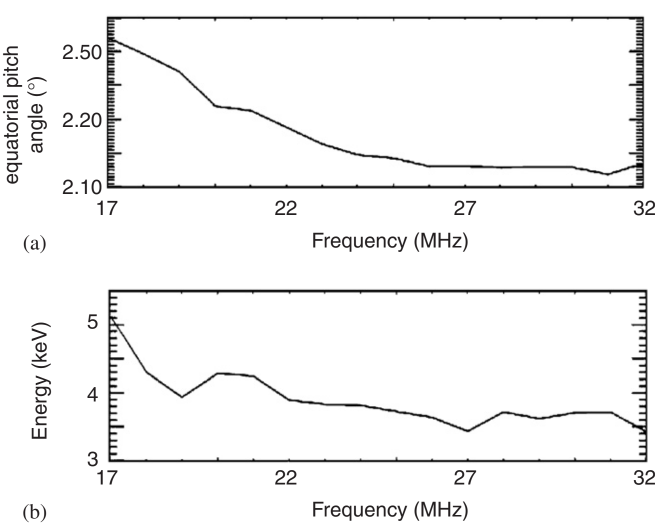

Fig. 8. Evolution of the emitting electrons characteristics with the frequency. (a) Averaged equatorial pitch angle as a function of the frequency $\langle\alpha_{eq}\rangle(f)$. (b) Averaged kinetic energy $\langle W\rangle(f)$.

(8) with respect to the rate of acceleration ε

$$\frac{\partial\alpha}{\partial\varepsilon}\sim\frac{1}{2(\mu-\varepsilon)}. \tag{9}$$

We can see that for lower energy (i.e. lower magnetic moment μ), the parallel acceleration (represented by ε) has more influence on the increase of the pitch angle. The pitch angle of more energetic electrons increases less than the pitch angle of electrons having a lower energy. Thus, the most energetic electrons are reflected at higher altitude (lower frequency) than the low-energy electrons, and the average electrons energy is expected to decrease with increasing frequencies, as observed.

6.2. Velocity distribution

From the total kinetic energy W and the first adiabatic invariant of the particles for each adiabatic segments, we can also compute the average parallel and perpendicular velocities $(v_\parallel, v_\perp)$ of the emitting electrons of each adiabatic segment at any given frequency (Eqs. (3) and (4)). We can thus get a statistical distribution of the velocities of the emitting electrons in the $(v_\parallel, v_\perp)$ frame at a given frequency.

Fig. 10a shows the distribution of the emitting electrons in the $(v_\parallel, v_\perp)$ frame at the altitude corresponding to a local cyclotron frequency of 20 MHz, i.e. just above the highest mirror points of the emitting electrons. In spite of the spread of the data over more than one year, the distribution has a simple structure. It has a straight border (dashed line) and is similar to a shifted "loss-cone" distribution. The shift corresponds to an excess of about 0.7 keV of parallel kinetic energy $W_\parallel$ on each adiabatic segment. This distribution seems consistent with the relation between kinetic energy W and mirror frequency of the emitting electrons introduced by an acceleration, as in Section 6.

Fig. 10b shows the distribution of the emitting electrons for dynamic spectra with at least one potential drop. Red dots show the velocities of electrons emitting the low-frequency segments (i.e. after deceleration), and the blue ones the high-frequency segments (i.e. before deceleration). The best-fit line (dashed) of blue dots crosses the origin of

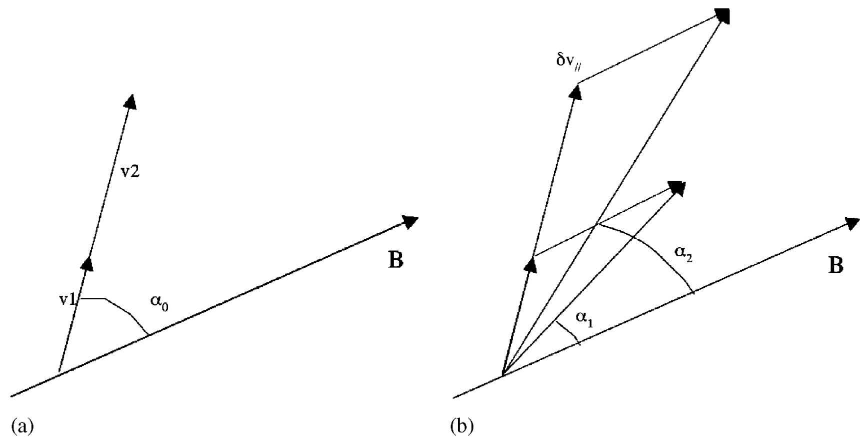

Fig. 9. (a) A parallel acceleration changes the pitch angle differently for fast or slow electrons. Initially the particles 1 and 2 whose velocities are v_1 and v_2 ($v_1 < v_2$) have the same pitch angle α_0. (b) A parallel acceleration adds a parallel velocity $\delta v_\parallel$ at each particle. The pitch angle of higher energy electrons vary less than the pitch angle of slow electrons. Thus, higher energy electrons have lower mirror frequency.

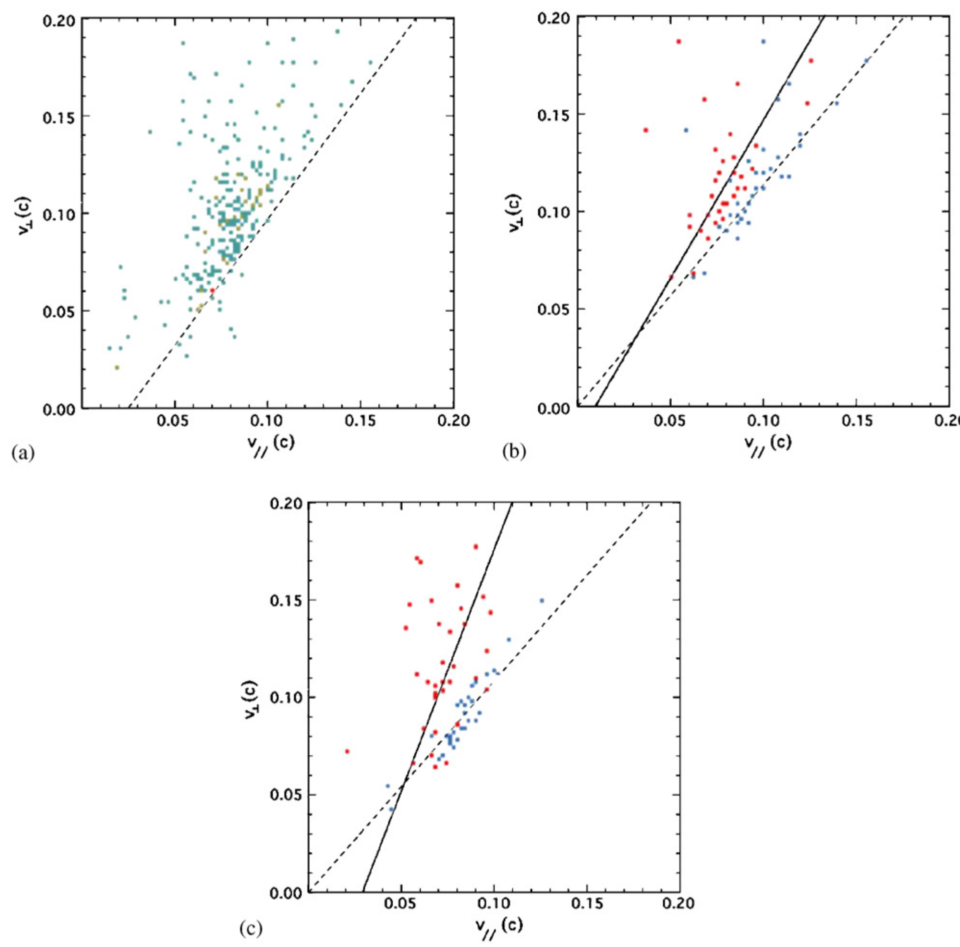

Fig. 10. (a) Measured velocity distribution of the electrons at an altitude corresponding to a cyclotron frequency of 20 MHz. This distribution is a shifted loss cone distribution. (b) Velocity distribution of the emitting electrons for the dynamic spectra which present potential drops. In red the low-frequency segments and in blue the high-frequency ones. Lines are linear fits to each cloud of points. (c) Velocity distribution of the emitting electrons for the dynamic spectra which present a single adiabatic segment. In red the segments at frequency below <22 MHz, in blue those above >28 MHz. Lines are quite similar to those of (b).

the $(v_\parallel, v_\perp)$ frame, i.e. the electrons emitting high-frequency segments have a velocity distribution which could be due to a loss cone (with mirror frequency about 36 MHz). The best fit of the red dots (continuous line) does not cross the origin, because decelerations shift electron velocities.

Fig. 10c shows the distribution of the emitting electrons for dynamic spectra with a single adiabatic segment. Red dots correspond to low-frequency segments (i.e. with mean frequency <22 MHz, below the potential drops frequency range) and blue ones to high-frequency segments (i.e. above >28 MHz). The best fit of these two clouds of points are quite similar to those of Fig. 10b, suggesting that red dots sustained decelerations, that could be due to small parallel potential drops and/or heating/cooling of the electrons. Adiabatic segments with intermediate frequencies (i.e. between 22 and 28 MHz) are not represented, they present an intermediate distribution mixing electrons decelerated and electrons reflected at the mirror point.

Finally, the "shifted-loss-cone" distribution in Fig. 10a can be interpreted to first order as the superposition of distributions of decelerated electrons whose deceleration before emission increases statistically with decreasing cyclotron frequency. It suggests the presence of structures decelerating the electrons between the surface and the emission altitude, even if we do not directly detect them.

7. Discussion

The study of the electrons parallel kinetic energy variations shows the presence of potential drops accelerating the emitting electrons toward Jupiter. We can distinguish two kinds of parallel accelerations: the large potential drops discussed in Section 5 and a more uniform acceleration (Section 2.5) modeled in this paper with the help of the rate ε.

Potential drops like those evidenced in Section 5 are observed in situ in the terrestrial auroral zones (Mozer et al., 1977). They are attributed to the presence of electrostatic double layers along the flux tubes (Block, 1978).

The presence of potential drops in IFT was expected, due to previous simulations showing abrupt variations of the potential near Jupiter. Solving the Vlasov and Poisson equations along the IFT, Su et al. (2003) found a potential drop of about 5 keV was found at $1.5R_J$. The localization and the amplitude of the simulated potential drop may vary with the choice of the boundary conditions in their simulation. The former were given by concentrations and velocity distributions of electrons and hydrogen, oxygen and sulfur ions both at the top of the Jovian ionosphere and in the Io torus. These parameters were estimated from in situ measurements of Voyager and Galileo. These simulations results are consistent with our detections of large potential drops (about 1 keV) near the Jovian ionosphere.

The acceleration acting more uniformly, modeled here with the parameter ε can be the consequence of smaller scale acceleration processes acting along a large portion of the Io–Jupiter flux tube. As the Io–Jupiter plasma has the structure of an Alfvén wing (Neubauer, 1980; Saur, 2004), we can expect that Alfvén waves play an important role in the acceleration of the electrons. Such acceleration processes have already been modelized in the conditions of the Earth auroral zone. The acceleration may be due, for instance, to small-scale Alfvén waves (Génot et al., 2004) encountering plasma density gradients, or to larger scale trapped Alfvén waves (Lysak and Song, 2003). Further studies are required to understand if these processes studied in the conditions of the Earth environment can also model the electron acceleration along the Io–Jupiter flux tube.

8. Conclusion

An automatic S-bursts recognition, identification and parallel energy calculation allowed us to confirm, with 5×10^6 measurements, the decrease of the drift at frequencies above 30 MHz, as first seen by Zarka et al. (1996). We confirm thus the average adiabatic motion of the electrons emitting the Jovian S-bursts with an energy of 4.5 ± 1.1 keV. Moreover, an automatic recognition of "adiabatic segments" in every dynamic spectrum permits an alternate validation of the adiabatic model over 230 individual dynamic spectra: bursts characteristics have been measured along each segment, providing for the first time the distribution of the energy and the equatorial pitch angle of the emitting electrons (Fig. 5). A mean energy of $W = 3.9\pm0.9$ keV and a mean equatorial pitch angle of $2.3^\circ\pm0.2^\circ$ are found. The error bars in Zarka et al. (1996) and in our Section 4.1 are thus due to the true dispersion of electron characteristics.

We observe for the first time the presence of 39 potential drops in the observed frequency range. These drops were expected by comparison with in situ observations of strong double layers in the Earth auroral zone and from electric potential simulations along the IFT but never observed. Ground-based S-bursts observations give us access to the distribution of amplitudes and localizations of these drops. Most of them are found in the range where Zarka et al. (1996) observed abrupt drift rate variations. Observations over several hours suggest (Fig. 7) that these potential drops build-up and last from minutes to tens of minutes.

The averaged energy decrease with frequency and the "integrated" velocity distribution of emitting electrons suggest a possible deceleration of the electrons in the vicinity of Jupiter, even if it is not directly observed.

Finally, this study shows the possibility to use ground-based radio observations to measure the characteristics of the IFT electrons and to probe the IFT electric potential structure with a resolution of a few hundred kilometres.

Acknowledgment

We gratefully thank Renée Prangé for her valuable suggestions on the velocity distribution study.

Appendix A. S-bursts recognition and drift rate analysis

The automated recognition of the S-bursts in a dynamic spectrum is done using a software developed by

LeGoff (1999). This software proceeds in two steps: First, the noise and the interference are eliminated from the dynamic spectrum. The sky background noise intensity presents at each frequency a Gaussian distribution with a standard deviation σ. Pixels of the dynamic spectrum for which intensity is less than 3σ are set to a null value. The acousto-optical recorder has a dynamic range of 25 dB. Thus Jovian emission, up to 30–40 dB above the background, may saturate part of the dynamic spectra. Saturate pixels and spectra are identified above a fixed threshold and set to zero. Broadband interference (lightning, etc.) and fixed frequency interference (human-made emissions) are also identified and eliminated.

Then the S-bursts are identified above the 3σ threshold defined earlier, and their pixels are set to unity and thus we get a binary image of the dynamic spectrum. The connected signal pixel clouds are identified and tagged as separate S-bursts.

The second step consists in eroding the burst signal in the dynamic spectrum image, in order to get its skeleton (i.e. to get a 1D shape curve). The skeleton obtained by erosion is refined through minimization of the so-called ''inertia'' of the skeleton, i.e. the quantity $\sum intensity \cdot distance^2$. The S-burst pixels are moved perpendicularly to the burst direction, following the intensity gradient. This operation increases the correlation between the skeletons and the dynamic spectrum. An example of skeletons computed from a dynamic spectrum is shown on Fig. 1. The recorded dynamic spectrum is presented in Fig. 1a and the skeletons of the recognized S-bursts in Fig. 1b.

From this skeleton we can compute the drift rate as a function of frequency. The drift rate is measured every 50 kHz for each S-burst. It is made by a linear regression on the skeleton in a frequency range of 0.5 MHz centered on each measurement frequency. The S-bursts can present a complex (multi-connected) topology. It is represented on the skeleton image by the split of the skeleton curve in two branches or more, each one with a different drift rate. Several drift rates are associated with the bifurcation point. The software automatically splits the bursts into elementary branches before computing the drift rates. Drift rate average and RMS dispersion is then computed at each frequency from all measurements at this frequency during the 20 s duration of the dynamic spectrum.

Drift rate computation is validated with a burst ''toy-model''. From the adiabatic model we compute the theoretical skeleton of a burst whose emitting electrons have a given kinetic energy and equatorial pitch angle. The theoretical drift rate is computed. Then we compute the drift rate from the skeleton using our software. The standard deviation due to the method is evaluated, and is found to be 1% of the drift rate measurement, much smaller than the average on every bursts of a dynamic spectrum.

References

Block, L.P., 1978. A double layer review. Astrophys. Space Sci. 55, 59–83.

Boischot, A., Rosolen, C., Aubier, M.G., Daigne, G., Genova, F., Leblanc, Y., Lecacheux, A., de La Noe, J., Moller-Pedersen, B., 1980. A new high-gain, broadband, steerable array to study Jovian decametric emission. Icarus 43, 399–407.

Carr, T.D., Desch, M.D., Alexander, J.K., 1983. Phenomenology of magnetospheric radio emissions. Physics of the Jovian Magnetosphere, Cambridge University Press, pp. 226–284.

Connerney, J.E.P., Acunã, M.H., Ness, N.F., Satoh, T., 1998. New models of Jupiter's magnetic field constrained by the Io flux tube footprint. J. Geophys. Res. 103 (12), 11929–11940.

Ellis, G.R.A., 1965. The decametric radio emission of Jupiter. Radio Sci. 69D, 1513–1530.

Ellis, G.R.A., 1974. The Jupiter radio bursts. Proc. Astron. Soc. Australia 2, 236–243.

Galopeau, P.H.M., Boudjada, M.Y., Rucker, H.O., 1999. Drift of jovian S-burst inferred from adiabatic motion in a parallel electric field. Astron. Astrophys. 341, 918–927.

Génot, V., Louarn, P., Mottez, F., 2004. Alfvén wave interaction with inhomogeneous plasmas: acceleration and energy cascade towards small-scales. Ann. Geophys. 6, 2081–2096.

Goldreich, P., Lynden-Bell, D., 1969. Io, a jovian unipolar inductor. Astrophys. J. 156, 59–78.

LeGoff, G., 1999. Analyse et reconnaissance des sursauts radio rapides de Jupiter dans le plan temps-fréquence. DEA Report, University of Cergy-Pontoise.

Louarn, P., 1992. Auroral planetary radio emissions—theoretical aspects. Adv. Space Res. 12, 121–134.

Lysak, R.L., Song, Y., 2003. Kinetic theory of the Alfvén wave acceleration of auroral electrons. J. Geophys. Res. (Space Phys.) 108 (A4), 1–6.

Mozer, F.S., Carlson, C.W., Hudson, M.K., Torbert, R.B., Parady, B., Yatteau, J., Kelley, M.C., 1977. Observations of paired electrostatic shocks in the polar magnetosphere. Phys. Rev. Lett. 38, 292–295.

Neubauer, F.M., 1980. Nonlinear standing Alfven wave current system at Io-theory. J. Geophys. Res. 85 (14), 1171–1178.

Queinnec, J., Zarka, P., 1998. Io-controlled decameter arcs and Io–Jupiter interaction. J. Geophys. Res. 103 (12), 26649–26666.

Riihimaa, J.J., 1991. Evolution of the spectral fine structure of Jupiter's decametric S-storms. Earth Moon Planets 53, 157–182.

Saur, J., 2004. A model of Io's local electric field for a combined Alfvénic and unipolar inductor far-field coupling. J. Geophys. Res. (Space Phys.) 109 (A18) 1210 − +.

Saur, J., Neubauer, F.M., Connerney, J.E.P., Zarka, P., Kivelson, M.G., 2004. Plasma interaction of Io with its plasma torus. Jupiter. The Planet, Satellites and Magnetosphere, Cambridge University Press, pp. 537–560.

Su, Y.-J., Ergun, R.E., Bagenal, F., Delamere, P.A., 2003. Io-related Jovian auroral arcs: modeling parallel electric fields. J. Geophys. Res. (Space Phys.) 108 (A2), 1–15.

Wu, C.S., Lee, L.C., 1979. A theory of the terrestrial kilometric radiation. Astrophys. J. 230, 621–626.

Zarka, P., Farges, T., Ryabov, B.P., Abada-Simon, M., Denis, L., 1996. A scenario for Jovian S-bursts. Geophys. Res. Lett. 23, 125–128.